Int J Appl Earth Obs Geoinformation 80 (2019) 257–267

Contents lists available at ScienceDirect

Int J Appl Earth Obs Geoinformation

journal homepage: www.elsevier.com/locate/jag

High-resolution mapping of biomass and distribution of marsh and forested wetlands in southeastern coastal Louisiana

Nathan Thomas[a,1,*], Marc Simard[e], Edward Castañeda-Moya[b,2], Kristin Byrd[c], Lisamarie Windham-Myers[d], Azure Bevington[b], Robert R. Twilley[b]

[a] CalTech Jet Propulsion Laboratory, Pasadena, CA, USA
[b] Department of Oceanography and Coastal Sciences, College of the Coast and Environment, Louisiana State University, Baton Rouge, LA, USA
[c] Western Geographic Science Center, U.S. Geological Survey, Menlo Park, CA, USA
[d] U.S. Geological Survey, Menlo Park, CA, USA
[e] Jet Propulsion Laboratory, California Institute of Technology, Pasadena, CA 91109, USA

1. Introduction

Coastal wetlands, both tidal and non-tidal, are composed of forested and woody shrub wetlands (e.g. swamps and mangroves) as well as emergent herbaceous vegetation, often referred to as marshes. These systems offer a plethora of important ecosystem services that include maintaining water quality, providing habitats for a variety of terrestrial and aquatic wildlife, storing carbon and mitigating against floods and coastal erosion (Mitra et al., 2005; Mitsch and Gosselink, 2007). Coastal wetlands produce and store organic carbon well in excess of ecosystem respiration and are considered critical sites for carbon burial, underscoring their significant contribution to carbon biogeochemistry in the coastal zone (Chmura et al., 2003; Mcleod et al., 2011). Along the northern Gulf of Mexico coast, Louisiana has one of the largest expanses of coastal wetlands, fed by the Mississippi River and its distributaries (i.e. the Atchafalaya River and Wax Lake Outlet). The Mississippi river has the seventh largest global water discharge and suspended load (Milliman and Meade, 1983; Meade, 1996), delivering sediment and organic detritus to these coastal wetlands. The annual quantity of sequestered C in the soil profile by vertical accretion is 2.96×10^6 metric tons, partially offset by losses of 1.86×10^6 (DeLaune and White, 2012). Despite the importance of Louisiana's wetlands, both locally and globally, their balance and sustainability has been altered as a consequence of natural processes and anthropogenic activities during the last century. A peak rate of wetland loss occurred in the 1970s at 10,200 ha $year^{-1}$ (Barras et al., 2003) contributing to a total loss of 4833 km^2 of marsh coverage, equitable to 25% of Louisiana's coastal wetlands (Couvillion et al., 2017). The marshes have been observed to be particularly vulnerable to loss due to their fragmented and isolated stands (Couvillion et al., 2016).

One detrimental influence upon the wetlands has been the limitation of over bank flow and sediment delivery to coastal wetlands due to the construction of flood control levees along the lower Mississippi River (Twilley et al., 2016). This has been exacerbated by canal construction, that has changed local wetland hydrology, combined with an increase in saltwater intrusion and wave erosion caused by relative sea level rise (Boesch et al., 1994). By the end of the century, sea level rise scenarios project between 218,897 ha and 587,527 ha of wetland will be lost in coastal Louisiana if lowest sea level rise scenarios or highest sea level rise scenarios are realized, respectively (Glick et al., 2013). The future of Louisiana's coastal wetland is dependent on whether sediment delivery from river discharge and organic accumulation are sufficient to sustain and allow wetland accretion at a rate as fast or faster than sea level rise (Paola et al., 2011). Provided that sufficient sediment is delivered into the wetlands during natural hydrologic conditions, soil elevation gain due to mineral (i.e. sediment deposition) and organic (i.e. plant production) accretion will contribute to land building and wetland expansion. This is currently occurring at the Wax Lake and Atchafalaya deltas; examples of progradational deltaic wetlands accreting at rates greater than sea level rise due to riverine sediment delivery (Roberts et al., 2003; Bevington et al., 2017). The impacts of reduced sediment inflow into the wetlands from the Mississippi River and sea level rise have been exacerbated by subsidence of the coastal zone as a result of the extraction of subsurface petrochemicals in the Gulf of Mexico (Morton et al., 2002, 2006). Episodic hurricanes and tropical storms in the region can cause wetland loss due to erosion (Barras, 2005) but they also deliver offshore sediments into coastal wetlands (Turner et al., 2006; Bevington et al., 2017). However, the long-term contribution of hurricane derived sediments to deltaic wetlands in the Wax Lake Delta was estimated to be only 22% of the long-term contribution of large river floods (Bevington et al., 2017), underlining the importance of riverine sediment in enabling the

* Corresponding author.
E-mail address: nathan.m.thomas@nasa.gov (N. Thomas).
[1] Present Address: Biospheric Sciences Laboratory, NASA Goddard Space Flight Center, Greenbelt, MD, USA.
[2] Present Address: Southeast Environmental Research Center, Florida International Univeristy, Miami, FL, USA.

https://doi.org/10.1016/j.jag.2019.03.013
Received 17 December 2018; Received in revised form 18 March 2019; Accepted 18 March 2019
Available online 07 May 2019
1569-8432/ © 2019 Elsevier B.V. All rights reserved.

wetland to maintain pace with sea level rise.

Given the importance of these coastal wetlands and the challenges that they face, reliable maps of the distribution and structure of wetland vegetation are of paramount importance. The wetlands of the United States are mapped as part of the National Oceanic and Atmospheric Administration (NOAA) Coastal Change Analysis Program (C-CAP dataset), produced in five-year intervals for the conterminous United States using Landsat 30 m pixel maps of coastal regions. The most recent C-CAP dataset (2010) was assessed to have an overall accuracy of 84% (McCombs et al., 2016). In addition, the U.S. Fish and Wildlife Service's National Wetlands Inventory (NWI) program has produced wetland maps for the conterminous United States. This has an effective date of the mid-1980s for states within the contiguous U.S, updated at a rate of 5% per year during the 1990s and which is currently reduced to a rate of 2%. These maps assign classes based on environmental setting by broadly defining and segregating wetlands based on salinity and water flow. This classification follows the A-16 land cover theme of the National Spatial Data Infrastructure (NSDI), mapping imprecise ecotones opposed to the explicit distribution of land cover type. This yields a higher ecological resolution at the expense of spatial resolution and the explicit extent of the marsh and forested wetlands. Recent maps distinguishing tidal marsh from non-tidal marsh extent only were attained by Byrd et al. (2018) by updating the C-CAP dataset and subsequently mapping an extent of 2228.7 km^2, while Couvillion et al. (2016) assessed the fragmentation of Louisiana coastal marshes. Using time-series Landsat data from 1985-2010, Couvillion et al. (2016) derived an aggregation index by assessing the pixels adjacent to vegetated pixels, revealing a decrease in aggregation in the marshes through time, particularly among the fragmented intermediate, brackish and saline marsh. Other more specific attempts at mapping the wetlands of Louisiana's wetlands have been in localized studies, focused on the comparison of remote sensing techniques (Ramsey and Laine, 1997) or quantifying post-hurricane changes in vegetation cover (Ramsey et al., 1997), without generating detailed land cover products. One of the aims of this study was to attain the definitive extent of the herbaceous marsh and forested wetlands in southeastern Louisiana.

Remote sensing provides a means of mapping and characterizing wetlands, which can be inaccessible or time consuming to document through field studies alone. The current rate and variety of remotely sensed data is unprecedented with freely available multispectral data available at 10 m spatial resolution. This is providing the opportunity to map wetland extent at high-resolution, although this has not yet been achieved for coastal Louisiana. Previous studies (Couvillion et al., 2016) have relied upon coarser imagery in order to benefit from the temporal resolution from successive sensors that have collected imagery over decadal periods, yet there is the opportunity to increase the accuracy of such datasets by using higher-resolution imagery and to begin a new time-series initiative that will be facilitated by forthcoming planned continuation missions. Existing maps of marsh extent have not utilized object-oriented methods that represent groups of pixels as meaningful parcels of land cover, despite their benefits of reducing pixelated noise in classifications and providing contextual information to the classifier (Gibbes et al., 2010; Blaschke, 2010). Similarly, increasingly popular machine learning algorithms that rely on fewer assumptions than existing algorithms have not been used to classify the Louisiana wetlands despite the demonstrated accuracy of their results (Fernández-Delgado et al., 2014). We aim to demonstrate the use of high-resolution imagery within an object-oriented machine learning approach for the mapping and classification of wetland extent. Coupled with field data, we use remote sensing to build upon the existing body of literature (Darby and Turner, 2008; Day et al., 2001; Hoeppner et al., 2008; Martin and Shaffer, 2005; Sasser et al., 1995) to provide wall-to-wall estimates of wetland coverage and biomass for southern Louisiana.

Estimations of AGB in southern Louisiana have primarily utilized *in situ* field plot data alone and the use of remote sensing has been limited. This has provided knowledge of species-specific patterns of AGB in discrete locations across Louisiana's coastal marshes but have not yielded single continuous wall-to-wall maps (DeLaune et al., 1979; Darby and Turner, 2008; Hopkinson et al., 1978; Day et al., 2001; Hoeppner et al., 2008). Field data has been coupled with remote sensing data but has either provided regional AGB estimates at very coarse resolution (Ghosh et al., 2016) or has focused on specific wetland types alone (Byrd et al., 2018). The ability to estimate AGB across the whole wetland is increasingly important as since 2017, coastal wetlands have been included in the Agriculture Forestry and Other Land Use (AFOLU) sector of the national greenhouse gas (GHG) inventory, following guidelines in the Intergovernmental Panel on Climate Change (IPCC) 2013 Wetlands Supplement (Hiraishi et al., 2014). Consequently, the carbon stock and changes in wetlands must be accounted for, across five carbon pools, including aboveground biomass. This accounting is aggregated into three tiers that range in complexity from the calculation of C emissions based on the area of loss multiplied by an emissions factor (tier 1), through to dynamic mechanistic-based models of CO_2-C emissions and dissolved organic carbon (DOC) export (tier 3). The combination of field and remotely sensed data, therefore, provides a potentially viable way of satisfying these requirements to inform a GHG inventory for the conterminous U.S.

2. Study site

The study area was confined to the Atchafalaya and Terrebonne coastal basins of Southern Louisiana within the Mississippi River Delta (MRD) floodplain (Fig. 1). The Mississippi Delta formed as a series of overlapping lobes over the past 6000–7000 years and consists of two physiographic units, the Deltaic plain to the east and Chenier plain to the west. The deltaic plain contains the Atchafalaya River, a major distributary of the Mississippi River that dominates the study site and which terminates at the Wax Lake and Atchafalaya deltas (Roberts, 1997). These deltas receive water and sediment discharge from the Atchafalaya River, which is maintained at 30% of the combined discharge of the Mississippi and Red Rivers. This discharge is managed by the U.S. Army Corps of Engineers at the Old River Control Structure. Atchafalaya Delta is regularly dredged for navigational purposes but Wax Lake Delta (WLD) has been left to accrete with little anthropogenic intervention. Subsequently, Wax Lake Delta is an excellent example of a prograding young deltaic system with prodelta deposits and subaqueous expansion first observed in 1952 (Wellner et al., 2005).

Herbaceous wetland vegetation in the Mississippi deltaic plain has previously been divided into nine vegetation types, differentiated by salinity (Visser et al., 1998). Alternatively, Sasser et al. (1996) describes five floating and one non-floating habitats based upon buoyancy dynamics, substrate characteristics and dominant vegetation, composed of 45 species within saline, brackish and fresh water marshes. Common species identified in the study area are *Spartina alterniflora*, *Spartina patens*, *Avicennia germinans*, *Juncus roemerianus*, *Distichlis spicata*, *Panicum hemitomon*, *Sagittaria lancifolia* and *Zizaniopsis miliacea*. Tree species are also present in the delta where cypress-tupelo swamps are dominated by *Taxodium distichum* (L.) Rich. baldcypress and *Nyssa aquatica* (L.) water tupelo. Additional woody species present are *Salix nigra* (L.), *S. interior* Rowlee and *Populus heterophylla* (L.) (Doyle et al., 1995).

3. Datasets

3.1. Sentinel-2

European Space Agency (ESA) Sentinel-2 data was downloaded from the USGS Earth Explorer platform. Sentinel-2 is a 13-band optical sensor that covers visible, near infrared and shortwave portions of the electromagnetic spectrum. The data is available as band dependent 10, 20 and 60 m resolution with a 290 km field of view. Sentinel-2 data is available via two platforms offering repeat pass data viewed at the same

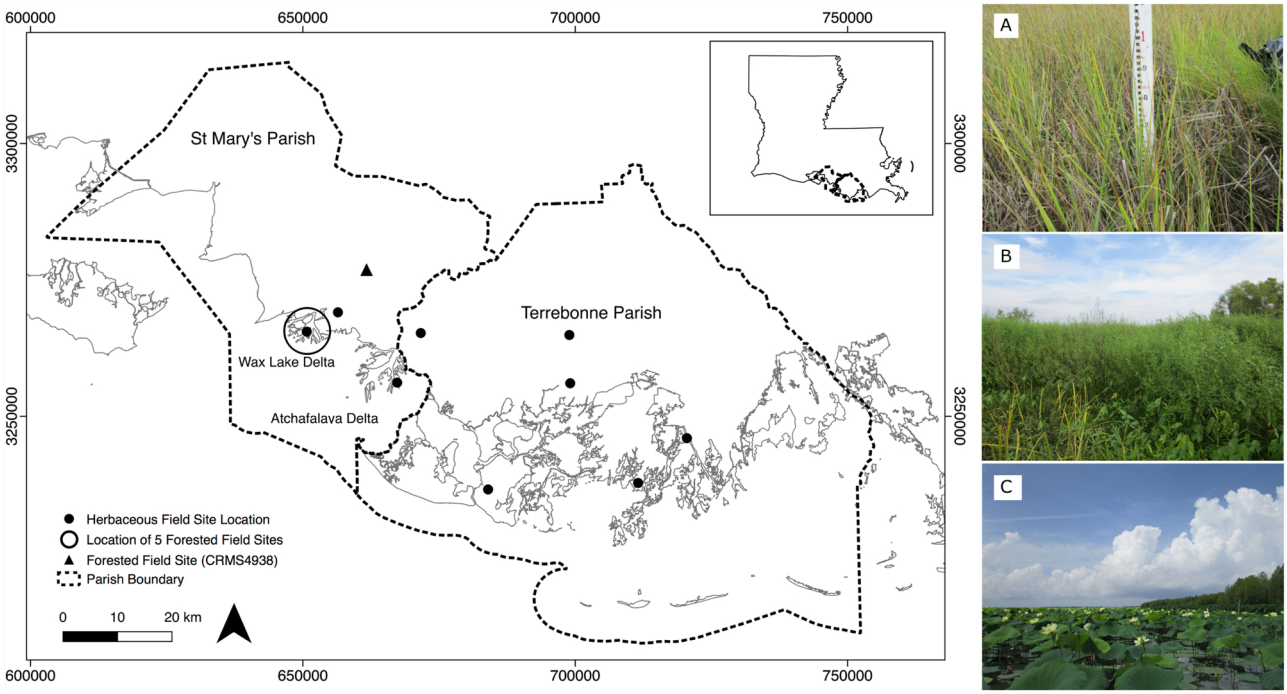

Fig. 1. Location of the study sites in the Atchafalaya and Terrebonne basins in southern Louisiana. Insets are field photographs of the typical vegetation found at the study site. (A) An example of *Spartina* which is common throughout the wetland. (B) An example of the dense cover and heterogeneity of the herbaceous marsh. (C) An example of floating vegetation at the study site.

angle every 5 days. A cloud free scene covering the entirety of the study area was acquired on September 8, 2017, during the period of seasonal peak biomass. The scene was acquired as 8 subsets and was corrected using the Dark Object Subtraction (DOS) algorithm using the Semi-Automatic Classification plugin (Gongedo, 2016) within QGIS. The scenes were mosaicked and then subset to the parish boundaries of St. Mary and Terrebonne.

3.2. Field data

A total of 15 wetland sites including forested wetlands (6 sites) and herbaceous wetlands (9) were selected across the Wax Lake/Atchafalaya delta complex (total of 8 sites) and West Terrebonne (total of 7 sites). Ten out of the 15 selected sites are part of the Coastal Reference Monitoring System (CRMS, Steyer et al. (2003)). Forested sampling sites were less accessible and were confined to the Wax Lake delta with the exception of one site that occurred at the location of a CRMS station. Two field campaigns (May and August 2015) were conducted to capture seasonal changes in biomass over the summer growing season, particularly for emergent herbaceous wetland sites. May is considered early phase of the growing season, whilst August–September, at the end of the growing season but before senescence, is considered the period of peak biomass. In forested sites, sampling was only conducted during May since changes in tree wood growth are very small and are difficult to detect over the four-month seasonal interval from May to August. At the forested wetland sites, duplicate circular plots (10 m radius; 50 m apart) were established inside the forest approximately 30 m from the edge. All trees with diameter at breast height (dbh, 1.3 m) $\geq$ 2.5 cm were measured within each plot and identified to species. The dominant species were willow trees, with lesser occurrences of baldcypress and maple. The height of all trees was measured with a laser range finder (Impulse 200 LR, Laser Technology Inc., Tucson, WY). Published species-specific allometric equations were used to estimate aboveground biomass (AGB) using Chojnacky et al. (2013) for willow and Jenkins et al. (2003, 2004) for baldcypress and maple. At the herbaceous wetland sites, a transect was established perpendicular to the wetland edge and AGB was harvested inside duplicate plots (0.25 $m^{-}2$; 5 m apart) established at 10, 50, and 100 m from the wetland edge. All AG plant material within each plot was clipped at their base to the ground level, stored in plastic bags and refrigerated before being transported and processed in the laboratory. Fresh plant material was initially sorted by species and subsequently dried for 72 h at 60 °C and weighed to obtain biomass. Aboveground biomass was expressed in g/m^2.

4. Methodology

4.1. Land cover classification

To classify wetland coverage within the St. Mary and Terrebonne parishes from Sentinel-2 imagery, four vegetation classes were chosen based upon the land cover types that could be differentiated in the Sentinel-2 imagery. Individual species and vegetation structural types could not be differentiated as they occurred in mixed stands that were below the pixel resolution of the imagery. This was confirmed through reference to the Coastal Reference Monitoring System (CRMS; Steyer et al. (2003)). Vegetation surveys at these locations revealed dominant and co-dominant species were able to account for almost equal proportions of cover. As the land cover and not species composition of the marsh was of interest, the marsh was represented as a single class. A forest class was included to account for the woody tree and shrub vegetation present. Additional classes of water and a joint class of unconsolidated sediment and impervious surfaces were also used. Water was masked using the Enhanced Vegetation Index (EVI) using a threshold of 0.1 but was included as a class to account for any remaining water pixels. The impact of tide was minimized as the imagery was acquired during a period of peak biomass when the marsh surface was dominated by vegetation and the presence of water in the pixels was reduced, particularly given the typically small tidal range (30 cm). As vegetation cover at the study site was sufficient enough to be sampled during a period of minimum biomass (May), by the summer (peak biomass) the increased vegetation cover limited the presence of any

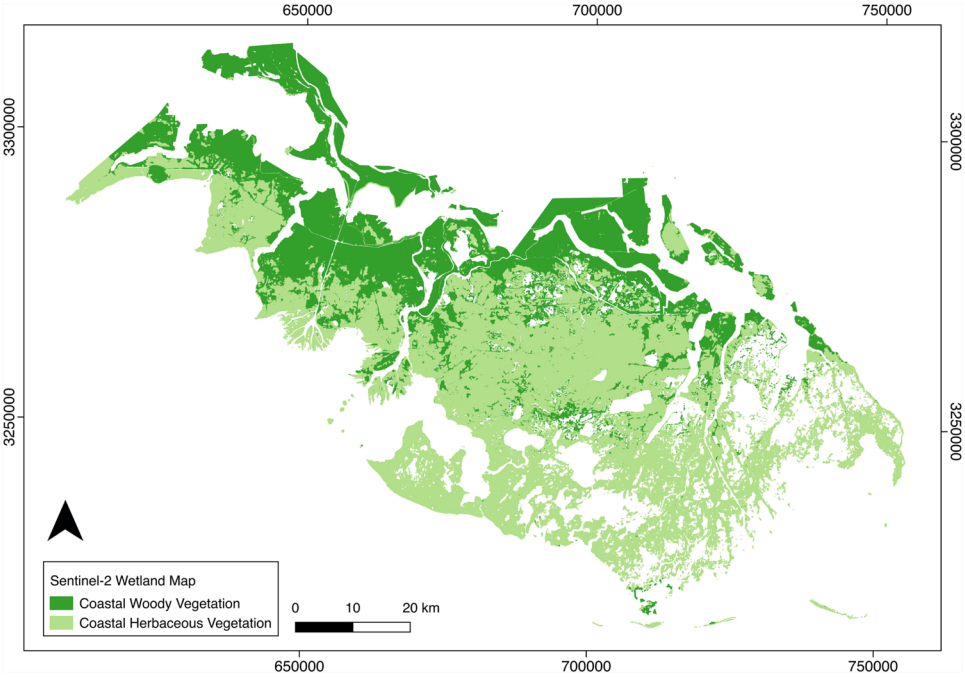

Fig. 2. Classification of coastal wetlands at the St. Mary and Terrebonne parishes, southern Louisiana from Sentinel-2 imagery. Woody and herbaceous vegetation dominate the western and central Wax Lake Delta and Atchafalaya Delta whilst herbaceous vegetation occupies the eastern portion of the study site and extend seawards. Among the herbaceous vegetation are levees covered by woody vegetation that line channels and the islands of the deltas.

water in the pixels. Agricultural areas were manually digitized and masked from the scenes prior to classification.

The Sentinel-2 imagery was segmented using the algorithm outlined in Clewley et al. (2014) within the Remote Sensing and GIS Library (RSGISLib, Bunting et al. (2014)) python module. The algorithm utilizes k-means clustering and iterative elimination of objects below a user defined size (10 pixels) to form image objects. The Sentinel-2 imagery was reprojected to a geographic coordinate system with a pixel spacing of approximately 5 m. This was done to aid the segmentation as the land cover types in the region often formed very small stands that were below the minimum segment size threshold (10 pixels). In order to avoid reducing the minimum object size so that it would yield a pixelated result, resampling the image allowed the minimum object size to remain high whilst capturing isolated portions of land cover. The resultant segmentation had an associated raster attribute table (RAT) that was populated with the mean input variable values. All of the Sentinel-2 reflectance bands, excluding the water vapor and cirrus bands were used as input variables. All of the near-infrared bands in the image were included as variables to determine whether a portion of the spectrum was most beneficial for classifying vegetation in this environment. To collect training samples, the segmentation was converted to a vector and was overlain over Google Earth imagery in QGIS. For each land cover class, image objects were selected and assigned a training class value. A total of 852 samples were chosen, distributed among four classes of woody vegetation (235), herbaceous vegetation (484), water (100) and bare earth/urban (33). The selection of the training polygons were selected using Google earth very-high-resolution imagery and with reference to the CRMS online database. All classes were readily separable in very-high-resolution imagery given the different structures of the vegetation types. These objects were subsequently rasterized and populated into the segmentation using the modal pixel value per object. This ensured that the majority training class value was assigned to the correct object, reducing the risk of incorrectly labeling a training object. None of the field collected samples were used as training inputs as information collected at a given plot could not be guaranteed to be representative of the entire associated image object. As a consequence of the marsh class being composed of a heterogeneous mixture of herbaceous species and vegetation structures, a non-parametric machine learning classifier was used. A Random Forest classifier was selected, having been demonstrated to out-perform other machine learning algorithms for remotely sensed datasets (Fernández-Delgado et al., 2014). The python scikit-learn (Pedregosa et al., 2011) implementation of Random Forests and open-source Geographic Object-Based Image Analysis (GEOBIA) approach used, is demonstrated in Clewley et al. (2014). An optimizer was used to derive the Random Forest parameters (1000 trees, 3 maximum features) which yielded an out-of-bag (oob) score for the classification of > 0.9. To validate the map, 1400 points were manually verified against high-resolution Google Earth imagery. Given the large area of the marsh and the forest classified, 500 points were validated for each vegetated class alongside 300 for the water class and 100 points for the unconsolidated/artificial surface class.

A comparison was made between the Sentinel-2 classified coverage and that of the NWI (2013) and C-CAP datasets (2010) which represent two of the most widely used datasets of Louisiana wetland extent. The NWI dataset is classified into the three classes of (1) Freshwater Forested/Shrub wetland, (2) Freshwater Emergent wetland and (3) Estuarine and Marine wetland. In order to form a comparison with the Sentinel-2 classification, the Freshwater Emergent wetland and Estuarine and Marine wetland classes were merged into a single marsh class. Similarly, the C-CAP classes were reclassified by merging palustrine emergent wetland, grassland and estuarine emergent wetland into a herbaceous vegetation class while palustrine forested wetland, palustrine scrub/shrub wetland and deciduous forest were merged into a single forest class. This reduced all of the classes in the existing maps into two categories representing woody and non-woody vegetation, for comparison with the Sentinel-2 classification. Given the different methods and resolutions used to derive the NWI and C-CAP datasets compared to the 2017 Sentinel-2 classification, a change map was not derived, however the existing maps were used as reference datasets to compare against our updated extent and to visualize where the greatest differences in the datasets occurred, highlighting areas of greatest potential change.

5. Results

5.1. Land cover map

The land cover map represents the most up-to-date extent of marsh and forested wetlands within the St. Mary and Terrebonne parishes of Southern Louisiana (Fig. 2). Forested wetlands were mapped within a

Table 1
Accuracy of 2017 Sentinel-2 land cover map.

	Water	Marsh	Bare	Forest	User (%)
Water	17	4.14	0	0.29	79.33
Marsh	0.07	33.5	0.14	2	93.8
Bare	0.21	0.21	6.71	0	94
Forest	0	2.43	0	33.29	93.2
Producer (%)	98.35	83.16	97.92	93.57	90.5
Accuracy (%)	90.5				

region north of the Wax Lake Delta and extended inland eastwards across the study site. The marsh dominated the southern and western portion of the study site. The Terrebonne parish had more marsh coverage than the St. Mary parish, where the coastal marsh occurred as a narrow band close to the coast. Conversely, the marsh coverage within the Terrebonne extended much further seaward and became fragmented into small isolated patches. Wax Lake Delta and Atchafalaya Delta were composed primarily of marsh with some areas of forested wetland. The marsh was the most dominant vegetation type covering 1751.4 ± 211.3 km^2 (59%) of the 2970 km^2 of vegetated area in the two parishes, excluding non-vegetated land cover types. Forested wetlands were almost as abundant, covering a total area of 1218.7 ± 149.9 km^2 (41%). The additional classes of Water and Bare surfaces accounted for 309.3 ± 6.75 km^2 and 30.3 ± 10.27 km^2, respectively. The map was assessed to have an overall accuracy of 90.5% (Table 1), with a quantity disagreement of 0.02 and allocation disagreement of 0.06. Quantity and allocation disagreement are indications of inaccuracy in terms of the area classified (quantity) and the spatial distribution of the inaccuracy (allocation), as outlined by Pontius and Millones (2011). Low quantity and allocation disagreement values support the overall accuracy of the classification. The error estimated for each class area was calculated following Olofsson et al. (2014).

Generated from higher resolution imagery, the Sentinel-2 derived wetlands extent map resolves a greater level of detail than that mapped in existing products. This provided a greater level of detail in a region which is a complex heterogeneous mixture of wetland vegetation types containing stands that were previously below available image resolution (i.e. Landsat). For instance, this was evident along the tree covered levees that border distributary channels and the deltaic islands (Fig. 3), which are often at or below the resolution of Landsat and were either poorly represented or omitted from existing maps. The total extent and distribution of the forested wetlands within these parishes has subsequently been unknown. As a result of this study their total areal extent is known, as well as their distribution among the wetlands, detailing the size and number of the stands, revealing the variation in structure of the vegetation across the parishes. It also enabled the fragmented wetlands in the Terrebonne parish to be more accurately defined as the boundary between the vegetation and the water was more readily separable. Knowledge on the extent of the marsh in these regions is critical, given their low elevation and increasing fragmentation and loss. This was a consequence of the effective 100 m^2 pixel area of Sentinel-2 in comparison to coarser 900 m^2 Landsat pixels. This increased spatial resolution offers a substantial improvement over existing maps as not only is the coverage of the wetlands updated, but the coverage of each class is better defined. This is exemplified in Fig. 3 that compares the Sentinel-2 wetlands map with that of the existing National Wetlands Inventory (NWI).

The Random Forest algorithm implementation determines the importance of the input variables in terms of their influence upon the land cover classification (Table 2). The most important variable was the blue band, closely followed by the shortwave infrared band. The near-infrared and red edge bands were ranked among the least important bands and were interpreted to be correlated with one another. To test this, the algorithm was run again with only one near-infrared band but the importance of the variable in the classifier remained low.

5.1.1. Comparison with existing wetland extent

A comparison between the NWI dataset and the Sentinel-2 classification is given in Fig. 4 and a comparison between the C-CAP and Sentinel-2 classification is given in Fig. 5. Differences between the datasets are expected, given the temporal range over which the datasets were produced and the different methods used for each. For example, estuarine wetlands were classified as such in C-CAP data on the criteria that total vegetation coverage was greater than 80%. This threshold can severely affect the coverage of the wetlands that C-CAP reports. The greatest difference between the existing maps and Sentinel-2 classification was in the extent of the marsh. The Sentinel-2 derived extent is much smaller than the NWI and C-CAP extents, particularly in the eastern portion of the study site. This difference was recognized as water in the sentinel-2 imagery and either removed by the watermask or classified as water, despite the imagery being collected during a period of peak biomass. This smaller extent is also visible on the seaward margins throughout the marsh. While the reasons for these discrepancies are unclear, they may be attributed to a potential loss in marsh, given that the differences are much greater than can be accounted for by the difference in pixel size. Furthermore, the classification accuracy was high, reducing the likelihood that this was due to classification error. The difference in marsh extent was considerably greater in the NWI than C-CAP dataset, particularly in the fragmented wetlands in the Terrebonne parish. Conversely, the Sentinel-2 derived extent is greater at Wax Lake Delta and Atchafalaya Delta, where the islands of the deltas are mapped in greater numbers and size than in previous datasets. This may represent the growth of the prograding deltas over time. The Wax Lake Delta and Atchafalaya Delta are not wholly included in the NWI dataset and are classified as unconsolidated sediment in the C-CAP dataset, which contribute to differences in marsh extent at these locations. Furthermore, the higher resolution Sentinel-2 map increased the quantity of forested wetlands, particularly in the parish of St. Mary, along the levees that line the distributaries in the marsh. These differences do not represent changes in the marsh with certainty, given the different methods and datasets used in their creation, but highlight that differences between the existing maps and the Sentinel-2 derived classification exist. Nevertheless, given the dynamic nature of the wetlands, differences due to potential changes in extent and composition must be considered. The differences between the areas of the classes are given in Table 3.

5.1.2. Biomass

Emergent herbaceous (onset and peak biomass season) marsh and forested wetland biomass estimates were achieved by aggregating the field sampled species into marsh and forested classes and averaging the biomass values. The small quantity of field sites prevented robust relationships between the field data and remotely sensed data being developed. The class averaged biomass values were applied to the corresponding class based on the land cover classification. This was exported to create a biomass density map for both May and September and was subsequently converted to a total quantity of biomass. The average biomass estimates in May for the herbaceous and woody classes were 381.83 g/m^2 and 22,702.3 g/m^2, respectively. The marsh wetland biomass densities increased in September to 797.69 g/m^2. The same woody vegetation measurements were used for both seasons, thus no increase in biomass was observed. The increased biomass values in September account for a larger total biomass (29,064,201.3 Mg) in the two parishes over May (28,335,916.6 Mg). The complete biomass statistics per class per season are provided in Table 4.

The total biomass of the forested wetlands was substantially larger than that of the herbaceous marsh area, given the much greater structural aboveground biomass of the trees and shrubs and the almost equitable area of the two classes within the study site. As expected, the

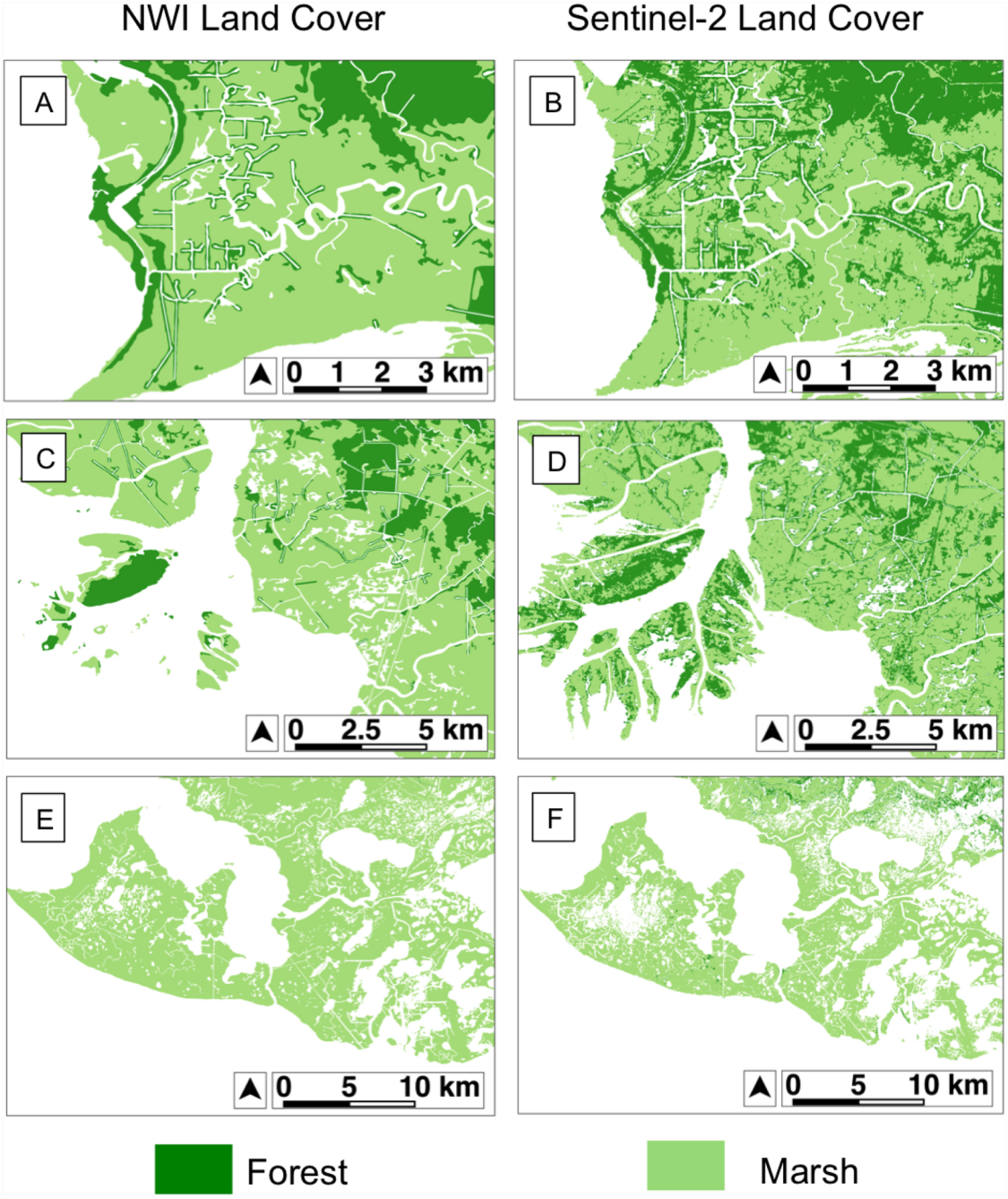

Fig. 3. Greater detail classified in the Sentinel-2 land cover map than existing national wetlands inventory (NWI) dataset at numerous locations across the study site. Forested wetlands are classified in more detail in the Sentinel-2 imagery than NWI dataset, alongside substantial differences in the extent of the herbaceous marsh. A, C and E are examples of the NWI map and B, D, and F demonstrate the increased detail classified at the same locations from Sentinel-2 imagery.

biomass of the herbaceous marsh was greater at the end of the growing season in September than in May, increasing by 108.9% over the growing season. The biomass estimates at each of the herbaceous sample sites is provided in Table 5, for both May and September, demonstrating the increase in average biomass for all except one plot location. The standard deviation values for the herbaceous and woody classes in May were 143.1 g/m^2 and 16,872.9 g/m^2, respectively. The September sampling of herbaceous aboveground biomass had a standard deviation of 248.1 g/m^2.

6. Discussion

6.1. Wetland extent

The Sentinel-2 derived land cover map provides the most up-to-date and detailed map of wetlands extent for southern coastal Louisiana within the parishes of St. Mary and Terrebonne. Land cover mapping of these wetlands has not been achieved at high spatial resolution over a geographical area as large as two parishes. Sentinel-2 imagery enabled a more detailed estimate of wetland area to be derived than from existing coarser maps of extent, to be used as a baseline for mapping subtle changes in the wetland extent as a consequence of loss events (e.g. hurricanes), or the increased progradtion of the deltas through

Table 2
The importance of each variable within the random forests classifier, as determined by the algorithm.

All variables	Score	Selected variables	Score
Blue	0.189	Shortwave infrared 2	0.246
Shortwave infrared 2	0.180	Blue	0.246
Red	0.128	Shortwave infrared	0.146
Shortwave infrared	0.116	Red	0.127
Green	0.097	Green	0.114
Red Edge 1	0.061	Near infrared	0.071
Coastal	0.055	Coastal	0.049
Narrow near infrared	0.047		
Near infrared	0.047		
Red edge 2	0.044		
Red edge 3	0.035		

sediment accumulation and organic matter production. The detection of these changes in coarser Landsat imagery may only be visible over a longer observation period due to the lower pixel resolution. The higher resolution also enabled smaller forested stands to be classified, particularly among the marsh wetland and along the leveed areas and prograding deltas. These forested patches are not represented well in existing datasets which are based upon coarser imagery, thus providing a less accurate extent map and class area estimate. The knowledge of such intricate details also provides additional important information, as the forested patches among the relatively newly formed deltas demonstrate that woody vegetation has become established in an otherwise dynamic region of the wetland. This reveals the high variability in the structure of the vegetation across the wetland, which was previously not known. This study provides more recent maps of wetland extent at higher resolution than available datasets such as the NWI and C-CAP land cover maps. Our study does not provide the same level of class specific information as these, but as such existing datasets are limited by being more broadly defined, composed of different vegetation types combined into single classes based on environmental conditions (e.g. salinity), based on the A-16 land cover theme of the NSDI (Cowardin et al., 1979). Our approach separates the woody from the herbaceous vegetation providing more accurate class extents at the expense of information on the surrounding environmental setting, thus providing a more detailed and accurate estimate of herbaceous marsh and forested wetland extent.

Here we provide a tractable means of attaining an independent up-to-date map of wetland coverage using a machine learning algorithm facilitated by a suite of open source data, software and tools. As an openly available dataset, Sentinel-2 was well positioned for mapping wetland extent in southern Louisiana, following examples of its use at other wetlands worldwide (Chatziantoniou et al., 2017; Pereira et al., 2017; Kaplan and Avdan, 2017). The 5-day return acquisition period for Sentinel-2 has the potential to allow the assessment of changes from episodic events (i.e. hurricanes and river floods) in this region, as well as providing a dense image archive to detect changes over longer periods, such as a result of sea level rise. As part of a constellation, imagery can be acquired at an unprecedented rate, providing the opportunity for a data-rich monitoring system of these important and dynamic wetlands, despite the occurrence of cloud cover. Furthermore, at Louisiana the large Sentinel-2 swath width was able to image the study site in one scene, negating the requirement to correct for temporal differences between adjacent scenes as with Landsat (Roy et al., 2016). Previous mapping efforts have contributed significant knowledge on wetland extent by measuring loss from published baselines and through using classification approaches and the visual interpretation of changes from existing land cover products (Barras et al., 2003; Day et al., 2000; Couvillion et al., 2011). Here, an object-oriented approach with a machine learning classifier differentiates our work from existing methods of estimating wetland extent, at the landscape scale. The ability to form image objects was beneficial in mapping the marsh extent by reducing pixelated noise and representing continuous land cover types as a single object. The use of Sentinel-2 within this approach was particularly effective at delineating the tree stands that lined the levees among the marsh and leading edge of the deltaic islands. In combination with a machine learning algorithm such as a random forest classifier, which relies on fewer assumptions of the training data than other parametric classifiers, we were able to achieve a classification accuracy in excess of 90%. The Random Forest classifier was able to represent multiple spectral classes under a single class label, which was particularly useful for combining heterogeneous pixels composed of many species into a single class. Our novel approach in the realm of applied earth observation for Louisiana's coastal wetlands can be readily exercised at any coastal region worldwide.

Changes in the wetland extent from existing maps could not be

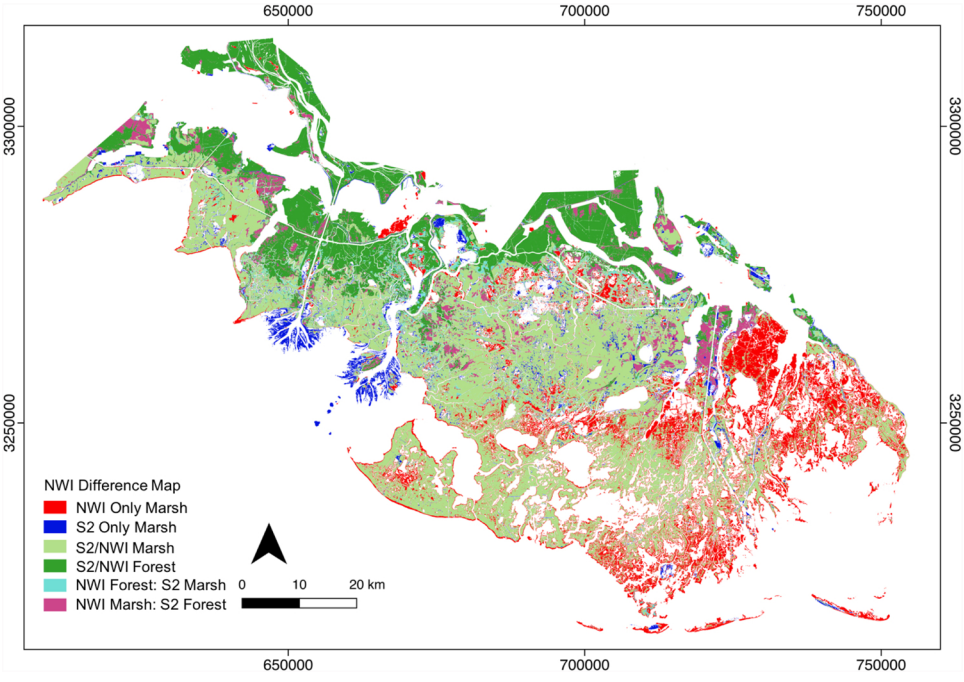

Fig. 4. Wetland area differences at the St. Mary and Terrebonne parishes, Louisiana between 2013 NWI and 2017 Sentinel-2. The red symbolizes marsh classified in the NWI dataset but not in this study. Blue represents additional marsh classified in 2017 Sentinel-2 imagery. Greens are marsh and forest classified in both datasets. Cyan is previously classified forest which is now classified as marsh (2017). The magenta is the inverse of the cyan. (For interpretation of the references to colour in this figure legend, the reader is referred to the web version of this article.)

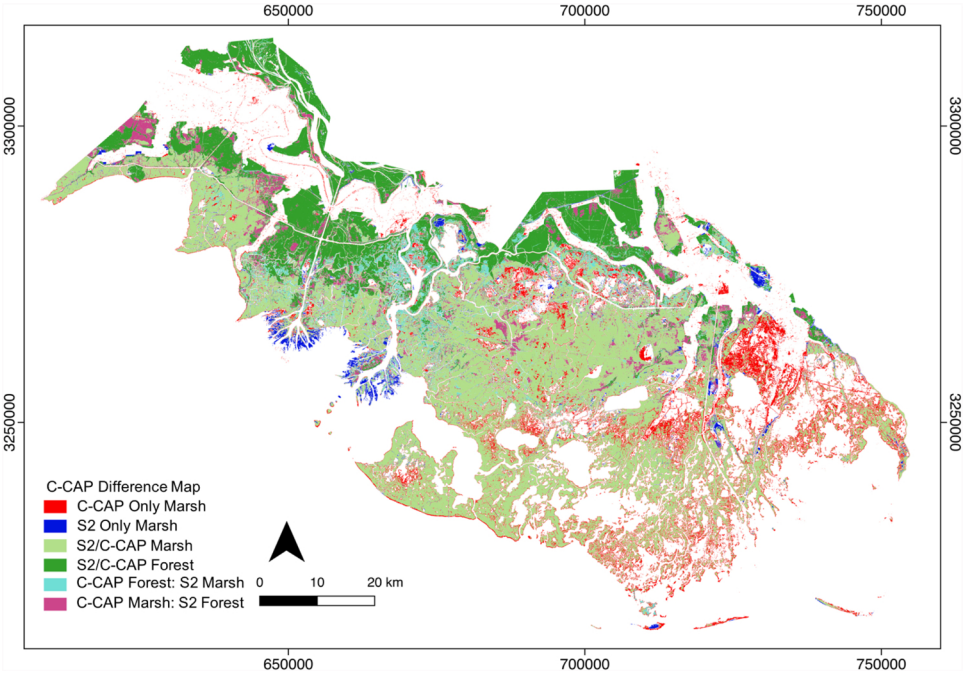

Fig. 5. Wetland area differences at the St. Mary and Terrebonne parishes, Louisiana between 2010 C-CAP and 2017 Sentinel-2. The red symbolizes marsh classified in the C-CAP dataset but not in this study. Blue represents additional marsh classified in 2017 Sentinel-2 imagery. Greens are marsh and forest classified in both datasets. Cyan is previously classified forest which is now classified as marsh (2017). The magenta is the inverse of the cyan. (For interpretation of the references to colour in this figure legend, the reader is referred to the web version of this article.)

reliably inferred although there are potential reasons for the observed differences in the Sentinel-2 classification. The large area of marsh mapped in the NWI/C-CAP dataset, but not classified in the Sentinel-2 map, could be due to a lack of sediment input into Terrebonne basin since it is disconnected from the river, causing the potential subsequent drowning of vegetation as the wetland is unable to accrete and maintain its extent. Saltwater intrusion has consequently been able to occur as a result of river abandonment and the migration of the marsh inland (Twilley et al., 2016). This is most noticeable within the marshes in the eastern portion of the Terrebonne Basin, where less marsh was classified around the perimeter of the isolated and fragmented marsh stands and where previously mapped marsh was now classified as water. This is supported by the observed decrease in aggregation amongst these brackish and saline marshes (Couvillion et al., 2016). The greater area of marsh classified at the deltas is consistent with increases in wetland coverage observed over the past 50 years (Twilley et al., 2016; Bevington and Twilley, 2018), however the majority of the additional marsh occurred at the Wax Lake Delta and Atchafalaya Delta, which were only partly included in the NWI datasets. The Wax Lake Delta is included in the C-CAP dataset but as non-vegetated unconsolidated sediment, despite being composed of both marsh and forested wetland types. It is possible that the C-CAP dataset mapped the Wax Lake Delta outside of the peak growing season when less vegetation was present. This study provides the most recent and high-resolution extent of the deltaic and coastal wetlands for this coastal area and will provide an extremely valuable baseline from which future measures of wetland area change can be compared to as part of the current restoration efforts in the region. Given the role that anthropogenic activity and the effects of climate change and sea level rise have on driving the observed loss and fragmentation of coastal wetlands in the region (Gagliano et al., 1981; Boesch et al., 1994; Barras et al., 2003; Couvillion et al., 2016), a detailed baseline of wetland coverage is critical for the monitoring of its response to restoration efforts and drivers of loss.

The coastal wetlands are comprised of a high diversity of vegetation types (e.g. herbaceous, grasses, shrubs, trees) that form mixed or monospecific stands of species that are below that of the comparatively coarse Sentinel-2 pixel resolution. This reduces the ability of Sentinel-2 to represent the heterogeneity of the marsh where there are no monospecific stands, thus the marsh could not be differentiated into species nor structure. A more detailed classification could be achieved through the use of very-high-resolution hyperspectral imagery (Carle et al., 2014), although this data is not readily available, is often limited in extent and requires extensive preprocessing (Jensen et al., 2017). However, the marsh and forest classes used in this study were readily and accurately separated in the Sentinel-2 imagery due to the distinct vegetation and plant cell structures. The reflection of near-infrared from plants is dominated by its scattering in between the cell-wall interfaces in the spongy mesophyll in addition to refractive discontinuities among other leaf components (e.g. protoplasts, stomata, cell membranes), as first observed by Gausman (1977). Visual discrimination between the marsh and forested wetlands was particularly prominent in the visible and near-infrared wavelengths, but were less discernible in the short-wave bands. This was juxtaposed with the variable importance derived from the Random Forest algorithm. The shortwave infrared band was the second most important variable whilst the near-infrared bands were among the least important. This was also true when only one near-infrared band was used, removing any potential correlation between the red edge and narrow near-infrared bands. A reason for this may be due to the higher detection of water content by the shortwave band, over the herbaceous wetlands. These have a less dense canopy than the forested wetlands which is disconnected from the flooded understory. The blue band was also deemed to be a consistently important variable in discriminating the wetland vegetation types. This could indicate the differences in the absorption of

Table 3
Comparison between marsh and forest extent classified in the Sentinel-2 (S2) derived map and the existing NWI and C-CAP extents.

	Additional S2 marsh (km^2)	Omitted S2 marsh (km^2)	Coincident marsh (km^2)	Coincident forest (km^2)	Marsh to S2 forest (km^2)	Forest to S2 marsh (km^2)
NWI	652	165.1	1567.5	797.7	141.7	238.3
C-CAP	526.1	109.5	1625.5	744	220.9	235.9

Table 4
Total biomass content of the marsh and forested wetlands. Densities are in grams per square meter (g/m^2) and total biomass is expressed in megagrams (Mg).

	Herbaceous emergent Wetlands			Forested wetlands (Sampled in May only)			Observed Wetland
	Mean (g/m^2)	StDev (g/m^2)	Study site total (Mg)	Mean (g/m^2)	StDev (g/m^2)	Study site total (Mg)	Total (Mg)
May 2015	381.83	143.09	668,684.5	22,702.25	16,872.85	27,667,232.1	28,335,916.6
September 2015	797.69	248.07	1,396,969.2	22,702.25	16,872.85	27,667,232.1	29,064,201.3
Seasonal change	415.86	NA	728,284.7	0.0	NA	0.0	728,284.7

Table 5
Change in aboveground biomass (AGB) for each herbaceous marsh sampling site over the growing season (May–September).

ID	Number of plots	May mean biomass (g/m^2)	September mean biomass (g/m^2)	Difference (g/m^2)	May SE (g/m^2)	September SE (g/m^2)
CRMS0301	1	125.96	1216.28	1090.32	0.00	0.00
CRMS0322	6	409.93	640.03	230.10	69.96	66.64
CRMS0465	6	387.29	682.60	295.31	36.39	74.95
CRMS6304	6	303.68	1015.80	712.12	100.13	92.57
Mike Island	6	347.17	612.63	265.45	27.51	107.19
CRMS0294	4	572.59	490.82	−81.77	130.85	93.33
CRMS0307	6	470.78	915.15	444.37	65.51	126.04
CRMS0411	6	260.60	591.55	330.95	19.54	36.91
CRMS0434	6	558.51	1014.40	455.89	100.13	92.57
Study site		381.83	797.69	415.86	47.70	82.71

chlorophyll-a between the two vegetation types. Similarly, the red band was the third most important variable and may indicate additional differences in chlorophyll-b also. These cannot be conclusively determined without the aid of further laboratory analysis or field spectroscopy.

6.2. Biomass

The seasonal increase in field measured biomass (108.9%) in the herbaceous wetland was a consequence of the vegetation attaining peak biomass over the summer growing season. Herbaceous vegetation is at maximum productivity during this period before senescing in late fall and winter. A seasonal increase in herbaceous biomass of over 100% at the sampling sites (Table 5) demonstrates the dynamic nature of these coastal wetlands, underscoring the influence of seasonality on wetland functioning in the region. The low standard deviation for the herbaceous wetland samples show little variation within the field collected biomass, with the larger standard deviation in September over May indicative of the increased variation in biomass during maximum biomass estimates, due to the differential biomass allocation strategies at the species level. The biomass standard deviation was large for the forest class, which was only measured in May, owing to the large range of values recorded in the field. The biomass values for the forest class occurred over a range of 5180–66,080 g/m^2, almost entirely within the same species. The wetland extent was mapped in this study during a period of peak biomass and therefore represents the maximum coverage and biomass of the marsh during September.

Previous estimates of aboveground biomass in the region have relied upon an *in situ* field plot sampling approach that allowed an understanding of species-specific patterns of aboveground biomass in several locations across Louisiana's coastal marshes (Martin and Shaffer, 2005; Sasser et al., 1996; Visser et al., 1998, 2017). Our study builds upon this to further our understanding on the spatial distribution of wetland biomass at the landscape level, using a combination of field measurements and remote sensing tools over the region. Recent studies have coupled remote sensing data with field data to model the biophysical attributes of the wetlands, expanding upon the use of field data alone. In instances where this was achieved over large areas, coarse MODIS data was used (Ghosh et al., 2016) while high spectral and spatial resolutions (1.2 m), which attain very detailed results, have been achieved for limited extents only (Mo et al., 2018). Additional work that has provided an updated extent of the wetland at the landscape scale has not used imagery of as high-resolution as Sentinel-2 and has focused on the estimation of the marsh wetland biomass, omitting the forested wetlands in the region (Byrd et al., 2018). The use of high-resolution Sentinel-2 imagery across a large geographical area has enabled a new estimation of aboveground biomass for the whole wetland at the landscape level, that is concurrent with previously published estimates of the wetland AGB Carpenter et al. (2007). Although we provide class averaged estimates of biomass, which are not species specific and do not account for the variability in biomass across the wetland outside of two forest and marsh classes, our estimates would be suitable for use within a framework for tier 1 reporting of GHG emissions. As the first wetlands inventory accounted for C stock changes in soil C alone, omitting the four other C pools (including AGB), this provides a tractable means of attaining the minimum requirement of the GHG inventory at Louisiana, which is applicable to all wetlands within the contiguous U.S. While access to the sampling sites is challenging, this study would benefit from additional field data which may reduce the standard error of the biomass estimations and facilitate relationships with remote sensing datasets to be developed. This may subsequently allow models of wetland biomass at a higher resolution to be generated and advance the estimates of AGB to meet the requirements of tier 2/3 of the GHG inventory.

7. Conclusion

In this study we generate estimates of marsh and forested wetland coverage and biomass within the Atchafalaya and Terrebonne coastal basins. ESA Sentinel-2 optical imagery was classified using a Random Forests machine learning algorithm within an open source geographic object based image analysis (GEOBIA) approach. A total area of 2950 km^2 of wetland was mapped with an accuracy in excess of 90%. We demonstrate the greater detail attained over existing maps with differences in coverage of 793.7 km^2. Field data collected during May and September 2015 provide seasonal mean herbaceous wetland biomass densities, ranging from 381.8 g/m^2 to 797.6 g/m^2, respectively. A mean woody biomass density for forested wetlands was estimated at 22,702.3 g/m^2. These values yielded a 108.9% increase in herbaceous wetland biomass over the growing season and a total wetland increase of 728,284.7 Mg for the two coastal basins. In this study we provide a tractable and repeatable means of mapping wetland coverage and

biomass into the future in southern Louisiana that is suitable for satisfying tier 1 requirements on the reporting of greenhouse gas emissions from wetlands, as outlined by the IPCC.

Acknowledgments

This study was funded by the NASA Carbon Monitoring System Program (NNH14AY67I). The field measurements also benefited from projects supported by the National Science Foundation via the National Center for Earth-Surface Dynamics (EAR-0120914), Frontiers of Earth Surface Dynamics (FESD, OCE-1135427), and the Coastal SEES program at LSU (EAR-1427389). This work was partly conducted by the Jet Propulsion Laboratory, California Institute of Technology, under contract with the National Aeronautics and Space Administration (NASA). This study benefited by having study sites associated with the long-term monitoring network maintained by Louisiana's Coastwide Reference Monitoring System (CRMS) Program. The CRMS Program is funded by the Coastal Wetland Planning, Protection, and Restoration Act Program and the State of Louisiana. We would like to thank all of the landowners who granted access to their properties to conduct this research, including Louisiana Department of Wildlife & Fisheries, Apache Corporation, ConocoPhillips, Continental Land & Fur, Emerald Land Corporation, Gruy Petroleum, Harry Bourg Corporation, and Miami Corporation. Special thanks to Sarai Piazza and Leigh Anne Sharp for providing technical guidance in accessing CRMS stations and landowner properties. The authors thank Alexandra Christensen, Annabeth McCall and Anika Aarons for assistance on field program management for this study and David Lagomasino for his helpful comments on the manuscript.

References

Barras, J., Beville, S., Britsch, D., Hartley, S., Hawes, S., Johnston, J., Kemp, P., Kinler, Q., Martucci, A., Porthouse, J., 2003. Historical and projected coastal Louisiana land changes: 1978–2050. U.S. Geol. Surv.

Barras, J.A., 2005. Land area changes in coastal Louisiana after Hurricanes Katrina and Rita. Science and the Storms: The USGS Response to the Hurricanes of 2005. pp. 98–113.

Bevington, A.E., Twilley, R.R., 2018. Island edge morphodynamics along a chronosequence in a prograding deltaic floodplain wetland. J. Coast. Res. 806–817.

Bevington, A.E., Twilley, R.R., Sasser, C.E., Holm, G.O., 2017. Contribution of river floods, hurricanes, and cold fronts to elevation change in a deltaic floodplain, northern Gulf of Mexico, USA. Estuar. Coast. Shelf Sci. 191, 188–200.

Blaschke, T., 2010. Object based image analysis for remote sensing. ISPRS J. Photogram. Rem. Sens. 65, 2–16.

Boesch, D.F., Josselyn, M.N., Mehta, A.J., Morris, J.T., Nuttle, W.K., Simenstad, C.A., Swift, D.J.P., 1994. Scientific assessment of coastal wetland loss, restoration and management in Louisiana. J. Coast. Res i-103.

Bunting, P., Clewley, D., Lucas, R.M., Gillingham, S., 2014. The Remote Sensing and GIS Software Library (RSGISLib). Comput. Geosci. 62, 216–226.

Byrd, K., Ballanti, L., Thomas, N., Nguyen, D., Holmquist, J., Simard, M., Windham-Myers, L., 2018. A remote sensing-based model of tidal marsh aboveground carbon stocks for the conterminous United States. ISPRS Photogram. Remote Sens (in press).

Carle, M.V., Wang, L., Sasser, C.E., 2014. Mapping freshwater marsh species distributions using WorldView-2 high-resolution multispectral satellite imagery. Int. J. Remote Sens. 35 (13), 4698–4716.

Carpenter, K., Sasser, C.E., Visser, J.M., DeLaune, R.D., 2007. Sediment input into a floating freshwater marsh: effects on soil properties, buoyancy, and plant biomass. Wetlands 27 (4), 1016–1024.

Chatziantoniou, A., Petropoulos, G.P., Psomiadis, E., 2017. Co-orbital Sentinel 1 and 2 for LULC mapping with emphasis on wetlands in a Mediterranean setting based on machine learning. Remote Sens. 9 (12), 1259.

Chmura, G.L., Anisfeld, S.C., Cahoon, D.R., Lynch, J.C., 2003. Global carbon sequestration in tidal, saline wetland soils. Global Biogeochem. Cycles 17.

Chojnacky, D.C., Heath, L.S., Jenkins, J.C., 2013. Updated generalized biomass equations for North American tree species. Forestry 87 (1), 129–151.

Clewley, D., Bunting, P., Shepherd, J., Gillingham, S., Flood, N., Dymond, J., Lucas, R., Armston, J., Moghaddam, M., 2014. A python-based open source system for geographic object-based image analysis (GEOBIA) utilizing raster attribute tables. Remote Sens. 6 (7), 6111–6135.

Couvillion, B., Beck, H., Schoolmaster, D., Fischer, M., 2017. Land area change in coastal Louisiana 1932 to 2016: U.S. Geological Survey Scientific Investigations Map 3381. Tech. Rep.Land area change in coastal Louisiana 1932 to 2016: U.S. Geological Survey Scientific Investigations Map 3381. Tech. Rep.

Couvillion, B.R., Barras, J.A., Steyer, G.D., Sleavin, W., Fischer, M., Beck, H., Trahan, N., Griffin, B., Heckman, D., 2011. Land Area Change in Coastal Louisiana from 1932 to 2010.

Couvillion, B.R., Fischer, M.R., Beck, H.J., Sleavin, W.J., 2016. Spatial configuration trends in coastal Louisiana from 1985 to 2010. Wetlands 36 (2), 347–359.

Cowardin, L.M., Carter, V., Golet, F.C., LaRoe, E.T., 1979. Classification of wetlands and deepwater habitats of the United States. Tech. Rep.Classification of wetlands and deepwater habitats of the United States. Tech. Rep.

Darby, F.A., Turner, R.E., 2008. Below-and aboveground biomass of *Spartina alterniflora*: response to nutrient addition in a Louisiana salt marsh. Estuar. Coasts 31 (2), 326–334.

Day, F.P., Crawford, E.R., Dilustro, J.J., 2001. Aboveground plant biomass change along a coastal barrier island dune chronosequence over a six-year period. J. Torrey Bot. Soc. 197–207.

Day, J.W., Britsch, L.D., Hawes, S.R., Shaffer, G.P., Reed, D.J., Cahoon, D., Britsch, L.D., Reed, D.J., Hawes, S.R., Cahoon, D., 2000. Pattern and process of land loss in the Mississippi Delta: a spatial and temporal analysis of wetland habitat change. Estuaries 23 (4), 425.

DeLaune, R.D., Buresh, R.J., Patrick, W.H., 1979. Relationship of soil properties to standing crop biomass of *Spartina alterniflora* in a Louisiana marsh. Estuar. Coast. Mar. Sci. 8 (5), 477–487.

DeLaune, R.D., White, J.R., 2012. Will coastal wetlands continue to sequester carbon in response to an increase in global sea level?.: a case study of the rapidly subsiding Mississippi river deltaic plain. Clim. Change 110 (1-2), 297–314.

Doyle, T.W., Keeland, B.D., Gorham, L.E., Johnson, D.J., 1995. Structural impact of Hurricane Andrew on the forested wetlands of the Atchafalaya Basin in south Louisiana. J. Coast. Res. 354–364.

Fernández-Delgado, M., Cernadas, E., Barro, S., Amorim, D., 2014. Do we need hundreds of classifiers to solve real world classification problems? J. Mach. Learn. Res. 15 (1), 3133–3181.

Gagliano, S.M., Meyer-Arendt, K.J., Wicker, K.M., 1981. Land loss in the Mississippi River deltaic plain. Gulf Coast Assoc. Geol. Soc. Trans. 31, 295–300.

Gausman, H.W., 1977. Reflectance of leaf components. Remote Sens. Environ. 6 (1), 1–9.

Ghosh, S., Mishra, D.R., Gitelson, A.A., 2016. Long-term monitoring of biophysical characteristics of tidal wetlands in the northern Gulf of Mexico – a methodological approach using MODIS. Remote Sens. Environ. 173, 39–58.

Gibbes, C., Adhikari, S., Rostant, L., Southworth, J., Qiu, Y., 2010. Application of object based classification and high resolution satellite imagery for Savanna ecosystem analysis. Remote Sens. 2 (dec 12), 2748–2772. URL http://www.mdpi.com/2072-4292/2/12/2748.

Glick, P., Clough, J., Polaczyk, A., Couvillion, B., Nunley, B., 2013. Potential effects of sea-level rise on coastal wetlands in Southeastern Louisiana. J. Coast. Res. 211–233 (Special Issue 63-Understanding and Predicting Charge in the Coastal Ecosystems of the Northern Gulf of Mexico).

Gongedo, L., 2016. Semi-Automatic Classification Plugin Documentation, Release 6.0.1.1.

Hiraishi, T., Krug, T., Tanabe, K., Srivastava, N., Baasansuren, J., Fukuda, M., Troxler, T.G., 2014. 2013 Supplement to the 2006 IPCC Guidelines for National Greenhouse Gas Inventories: Wetlands. IPCC, Switzerland.

Hoeppner, S.S., Shaffer, G.P., Perkins, T.E., 2008. Through droughts and hurricanes: tree mortality, forest structure, and biomass production in a coastal swamp targeted for restoration in the Mississippi River Deltaic Plain. For. Ecol. Manage. 256 (5), 937–948.

Hopkinson, C.S., Gosselink, J.G., Parrando, R.T., 1978. Aboveground production of seven marsh plant species in coastal Louisiana. Ecology 59 (4), 760–769.

Jenkins, J.C., Chojnacky, D.C., Heath, L.S., Birdsey, R.A., 2003. National-scale biomass estimators for United States tree species. For. Sci. 49 (1), 12–35.

Jenkins, J.C., Chojnacky, D.C., Heath, L.S., Birdsey, R.A., 2004. Comprehensive Database of Diameter-based Biomass Regressions for North American Tree Species, Gen. Tech. Rep. NE-319. US Department of Agriculture, Forest Service, Northeastern Research Station, Newtown Square, PA p. 45 [1 CD-ROM].

Jensen, D.J., Simard, M., Cavanaugh, K.C., Thompson, D.R., 2017. Imaging spectroscopy BRDF correction for mapping Louisiana's Coastal Ecosystems. IEEE Trans. Geosci. Remote Sens.

Kaplan, G., Avdan, U., 2017. Mapping and monitoring wetlands using SENTINEL-2 satellite imagery. ISPRS Ann. Photogram. Remote Sens. Spatial Inform. Sci. 271–277.

Martin, S.B., Shaffer, G.P., 2005. Sagittaria biomass partitioning relative to salinity, hydrologic regime, and substrate type: implications for plant distribution patterns in coastal Louisiana, United States. J. Coast. Res. 167–174.

McCombs, J.W., Herold, N.D., Burkhalter, S.G., Robinson, C.J., 2016. Accuracy assessment of NOAA coastal change analysis program 2006–2010 land cover and land cover change data. Photogram. Eng. Remote Sens. 82 (9), 711–718.

Mcleod, E., Chmura, G.L., Bouillon, S., Salm, R., Björk, M., Duarte, C.M., Lovelock, C.E., Schlesinger, W.H., Silliman, B.R., 2011. A blueprint for blue carbon: toward an improved understanding of the role of vegetated coastal habitats in sequestering CO_2. Front. Ecol. Environ. 9 (10), 552–560.

Meade, R.H., 1996. River-sediment inputs to major deltas. Sea-level Rise and Coastal Subsidence. Springer, pp. 63–85.

Milliman, J.D., Meade, R.H., 1983. World-wide delivery of river sediment to the oceans. J. Geol. 1–21.

Mitra, S., Wassmann, R., Vlek, P.L.G., 2005. An appraisal of global wetlands area and its organic carbon stock. Curr. Sci. 25–35.

Mitsch, W.J., Gosselink, J.G., 2007. In: Hoboken (Ed.), Wetlands. John Wiley & Sons, Inc.

Mo, Y., Kearney, M.S., Riter, J.C.A., Zhao, F., Tilley, D.R., 2018. Assessing biomass of diverse coastal marsh ecosystems using statistical and machine learning models. Int. J. Appl. Earth Observ. Geoinform. 68, 189–201.

Morton, R.A., Bernier, J.C., Barras, J.A., 2006. Evidence of regional subsidence and associated interior wetland loss induced by hydrocarbon production, Gulf Coast Region, USA. Environ. Geol. 50 (2), 261–274.

Morton, R.a., Buster, N.a., Krohn, M.D., Ruppel, S., 2002. Subsurface controls on historical subsidence rates and associated wetland loss in Southcentral Louisiana. Trans. Gulf Coast Assoc. Geol. Soc. 52 (2), 767–778.
Olofsson, P., Foody, G.M., Herold, M., Stehman, S.V., Woodcock, C.E., Wulder, M.A., 2014. Good practices for estimating area and assessing accuracy of land change. Remote Sens. Environ. 148, 42–57.
Paola, C., Twilley, R.R., Edmonds, D.A., Kim, W., Mohrig, D., Parker, G., Viparelli, E., Voller, V.R., 2011. Natural processes in delta restoration: application to the Mississippi Delta. Annu. Rev. Mar. Sci. 3, 67–91.
Pedregosa, F., Varoquaux, G., Gramfort, A., Michel, V., Thirion, B., Grisel, O., Blondel, M., Prettenhofer, P., Weiss, R., Dubourg, V., 2011. Scikit-learn: machine learning in Python. J. Mach. Learn. Res. 12, 2825–2830.
Pereira, O.J.R., Melfi, A.J., Montes, C.R., 2017. Image fusion of Sentinel-2 and CBERS-4 satellites for mapping soil cover in the wWetlands of Pantanal. Int. J. Image Data Fusion 8 (2), 148–172.
Pontius Jr., R.G., Millones, M., 2011. Death to Kappa: birth of quantity disagreement and allocation disagreement for accuracy assessment. Int. J. Remote Sens. 32 (15), 4407–4429.
Ramsey III, E.W., Laine, S.C., 1997. Comparison of Landsat Thematic Mapper and high resolution photography to identify change in complex coastal wetlands. J. Coast. Res. 281–292.
Ramsey Ill, E.W., Chappell, D.K., Baldwin, D.G., 1997. AVHRR imagery used to identify hurricane damage in a forested wetland of Louisiana. Photogram. Eng. Remote Sens. 63 (3), 293–297.
Roberts, H.H., 1997. Dynamic changes of the Holocene Mississippi River delta plain: the delta cycle. J. Coast. Res. 605–627.
Roberts, H.H., Coleman, J.M., Bentley, S.J., Walker, N., 2003. An embryonic major delta lobe: a new generation of delta studies in the Atchafalaya-Wax Lake Delta system. Gulf Coast Assoc. Geol. Soc. Trans. 53, 690–703.
Roy, D.P., Zhang, H.K., Ju, J., Gomez-Dans, J.L., Lewis, P.E., Schaaf, C.B., Sun, Q., Li, J., Huang, H., Kovalskyy, V., 2016. A general method to normalize Landsat reflectance data to nadir BRDF adjusted reflectance. Remote Sens. Environ. 176, 255–271.
Sasser, C.E., Gosselink, J.G., Swenson, E.M., Swarzenski, C.M., Leibowitz, N.C., 1996. Vegetation, substrate and hydrology in floating marshes in the Mississippi River Delta Plain wetlands, USA. Vegetatio 122 (2), 129–142.
Sasser, C.E., Visser, J.M., Evers, D.E., Gosselink, J.G., 1995. The role of environmental variables on interannual variation in species composition and biomass in a subtropical minerotrophic floating marsh. Can. J. Bot. 73 (3), 413–424.
Steyer, G.D., Sasser, C.E., Visser, J.M., Swenson, E.M., Nyman, J.A., Raynie, R.C., 2003. A proposed coast-wide reference monitoring system for evaluating wetland restoration trajectories in Louisiana. Coastal Monitoring through Partnerships. Springer, pp. 107–117.
Turner, R.E., Baustian, J.J., Swenson, E.M., Spicer, J.S., 2006. Wetland sedimentation from hurricanes Katrina and Rita. Science 314 (5798), 449–452.
Twilley, R.R., Bentley, S.J., Chen, Q., Edmonds, D.A., Hagen, S.C., Lam, N.S.-N., Willson, C.S., Xu, K., Braud, D., Hampton Peele, R., McCall, A., 2016. Co-evolution of wetland landscapes, flooding, and human settlement in the Mississippi River Delta Plain. Sustain. Sci. 11 (4), 711–731.
Visser, J., Duke-Sylvester, S.M., Shaffer, G.P., Hester, W.W., Couvillion, B., Broussard, W.P.I., Willis, J.M., Beck, H., 2017. In: 2017 Coastal Master Plan: Attachment C3-5: Vegetation. Version Final, Tech. Rep. Coastal Protection and Restoration Authroity, Baton Rouge, Louisiana.
Visser, J.M., Sasser, C.E., Chabreck, R.H., Linscombe, R.G., 1998. Marsh vegetation types of the Mississippi River deltaic plain. Estuaries 21 (4), 818–828.
Wellner, R., Beaubouef, R., Van Wagoner, J., Roberts, H., Sun, T., 2005. Jet-plume depositional bodies-the primary building blocks of Wax Lake Delta. Gulf Coast Assoc. Geol. Soc. Trans. 55.